Cell Communication and Signaling

RESEARCH

Open Access

Inhibition of tubular epithelial cells ferroptosis alleviates renal interstitial fibrosis by reducing lipid hydroperoxides and TGF-β/Smad signaling

Yuting Chen[1,2,3†], Yue Dai[1,2†], Yi Huang[1,2], Le Zhang[1,2], Cuntai Zhang[1,2], Hongyu Gao[1,2*] and Qi Yan[1,2*]

Abstract

Background Ferroptosis is a non-apoptotic form of regulated cell death that involves an imbalance in the homeostasis of two elements: iron and lipid hydroperoxides. The accumulation of lipid hydroperoxide serves as a key trigger for initiating ferroptosis. Recent studies have identified ferroptosis as a critical pathophysiology contributing to kidney disease progression. However, the specific mechanisms underlying the role of ferroptosis in chronic kidney disease (CKD) have not been elucidated.

Methods Tubular epithelial cells (TECs) ferroptosis was evaluated in unilateral ureteral obstruction (UUO) models and in TGF-β-treated HK-2 cells to explore the relationship between ferroptosis and fibrosis. Ferroptosis inhibitors (ferrostatin-1) and TECs-targeted glutathione peroxidase 4 (GPX4) overexpression in vivo and in vitro were used to investigate the effect and mechanism of TECs ferroptosis on fibrosis progression.

Results Our findings indicate that ferroptosis is persistently activated during various states of the UUO model. As the results, ferroptosis was identified as a core facilitator of renal interstitial fibrosis in TECs during UUO. The reduction in TECs ferroptosis significantly ameliorated renal fibrosis and maintained the structure in the proximal tubules. Persistent activation of TECs ferroptosis effectively aggravated fibrosis progression through the TGF-β/Smad pathway.

Conclusions Inhibiting ferroptosis effectively rescues the accumulation of profibrotic cytokines, thereby alleviating renal fibrosis. The profibrotic mechanism of ferroptosis is closely related to the TGF-β/Smad pathway, and targeting ferroptosis and increasing GPX4 expression could be an effective strategy for treating CKD.

Keywords Renal interstitial fibrosis, Ferroptosis, Lipid hydroperoxide, Tubular epithelial cells, Pro-fibrotic factors

†Yuting Chen and Yue Dai contributed equally to this work.

*Correspondence:
Hongyu Gao
hygao@tjh.tjmu.edu.cn
Qi Yan
yanqi@tjh.tjmu.edu.cn
Full list of author information is available at the end of the article

Graphical Abstract

The occurrence of TECs ferroptosis in CKD is due to an imbalance in iron and lipid regulation, which drives the occurrence of lipid peroxidation and the accumulation of lipid hydroperoxide. One of the primary drivers of ferroptosis, lipid peroxidation, further stimulates TGF-β/Smad signaling and exacerbates fibrosis progression. Abbreviations: TFRC, transferrin receptor protein 1; DMT1, divalent metal transporter 1; FPN, ferroportin; ACSL4, acyl-CoA synthetase long-chain family 4; LPCAT3, lysophosphatidylcholine acyltransferase 3; GPX4, glutathione peroxidase 4; CTGF, connective tissue growth factor; PDGFB, platelet-derived growth factor subunit b; FGF2, fibroblast growth factor 2; TECs, tubular epithelial cells; CKD, chronic kidney disease. (The figure was drawn with BioRender.)

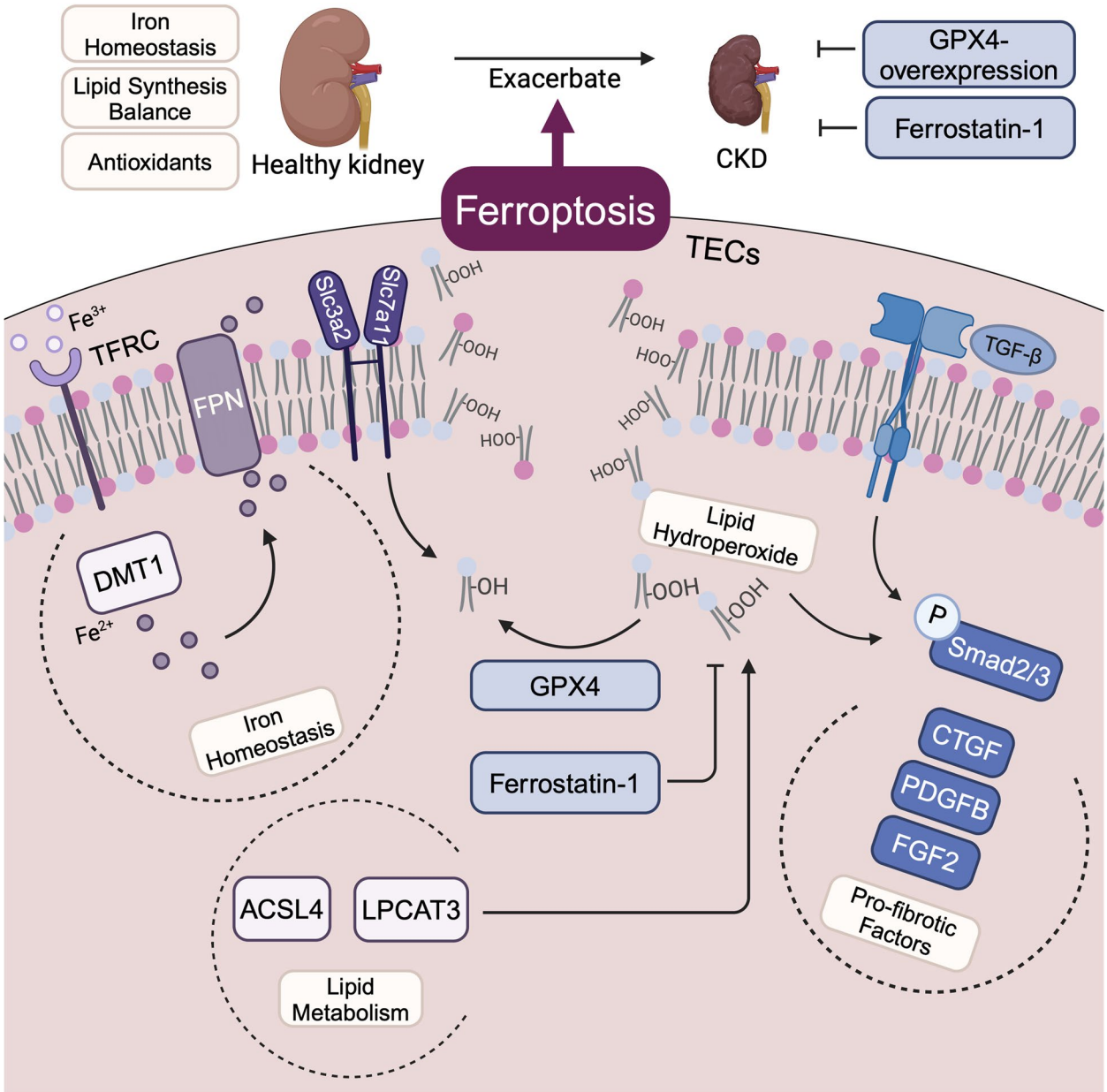

Introduction

Kidney diseases are becoming major health issues in modern society [1, 2]. Although kidney lesions are specific to the potential etiology of a particular kidney disease, fibrosis shows almost identical manifestations in all progressive forms of chronic kidney disease (CKD), indicating that it is a final common pathway in this condition [3]. Access to and effectiveness of treatments for CKD are currently limited. Kidney tubular epithelial cell (TEC) death is a key event in CKD caused by hypoxia, oxidative stress, mechanical injury, and senescence [4]. Multiple cell death pathways are involved in CKD, but the mechanism by which renal fibrosis is regulated by other non-apoptotic forms of regulated cell death has not been completely elucidated. Thus, the optimal therapeutic strategy remains unclear.

Ferroptosis is a form of programmed cell death characterized by the communication of lipid hydroperoxides in an iron-dependent manner [5, 6]. Ferroptotic cell death is morphologically, biochemically, and genetically distinct from apoptosis, various forms of necrosis, and autophagy [7]. Ferroptosis plays a crucial role in the development and disease of various organisms, including ischemia–reperfusion injury (IRI), cancer, and neurodegeneration [6, 8]. In 1996, the study has shown that excess iron in TECs can lead to kidney injury [9]. Subsequently, it is also found in CKD that the iron overload in TECs and leads to fenton reaction, which aggravating the process of renal fibrosis [10]. Treatment with the iron chelator DFO can effectively reduce iron accumulation in TECs and improve the progression of renal fibrosis [11]. According to the forefront studies in ferroptosis, the main sources of lipid hydroperoxides that cause ferroptosis are not only relate to fenton reaction, but also depend on lipid peroxidation which is caused by oxidative stress and lipid metabolism disorders [12]. Furthermore, our previous study revealed that specific inhibition of lipid metabolism effectively alleviates TECs ferroptosis and helps to rescue the fibrotic process during UUO [13]. Therefore, the inhibition of ferroptosis has been considered as an effective strategy for alleviating the fibrotic process in the kidney [14–16].

Glutathione peroxidase 4 (GPX4), a selenium-containing enzyme, plays a crucial role in reducing phospholipid hydroperoxides (PL-OOH) in mammalian cells. Conditional knockout studies of GPX4 provided the first evidence of a previously unrecognized form of cell death characterized by unrestrained lipid peroxidation [17]. The concept of ferroptosis as an iron-dependent cell death pathway was later introduced through the detailed characterization of the lethal mechanisms of erastin and (1 S, 3R)-RSL3 (RSL3) [5], which target system xc^- and GPX4, respectively [18]. Since then, the cysteine/GSH/GPX4 axis has been recognized as the central regulator of ferroptosis [19]. Moreover, although Friedmann Angeli [19] et al. provided direct evidence that inducible disruption of GPX4 causes acute renal failure, the precise mechanism by which GPX4 influences ferroptosis in fibrotic kidneys remains unclear.

In this study, we investigated the role of ferroptosis in renal interstitial fibrosis in vivo and in vitro. We explored the temporal relationship between ferroptosis and renal interstitial fibrosis by constructing a UUO model at 3, 7 and 14 days. Ferroptosis was ameliorated through pharmacological inhibition with ferrostatin-1 (Fer-1) and TEC-targeted GPX4 overexpression, which demonstrated the profibrotic role of ferroptosis in vivo and in vitro. Mechanistically, we demonstrated that ferroptosis in TECs promoted kidney fibrosis via TGF-β/Smad signaling and increased the production of various profibrotic factors, such as TGF-β, CTGF, PDGFB, and FGF2. Consistently, the profibrotic signals were reduced in response to both ferrostatin-1 and GPX4 overexpression.

Results

Ferroptosis persistently occurs in tubular epithelial cells during UUO

To explore the temporal relationship between ferroptosis and renal fibrosis, we tested ferroptosis in C57BL/6 mice subjected to UUO at 3, 7, and 14 days (Fig. 1a). The results demonstrated that ferroptosis in renal TECs was evident at 14 days, consistent with our previous study [13]. To examine the degree of ferroptosis in the UUO model, lipid peroxidation indicators were characterized by immunofluorescent expression of 4-hydroxynonenal

(See figure on next page.)

Fig. 1 Ferroptosis is persistently activated in TECs during UUO. **a** UUO was conducted in C57BL/6 mice, which were sacrificed 3, 7 or 14 days after obstruction. Sham mice were included as controls. **b** Representative immunostaining images ($n=5$) of lipid peroxidation-associated markers (4-HNE) in mouse kidney biopsy samples. Scale bars, 50 μm. **c** Western blot analysis of GPX4, ACLS4, and LPCAT3 expression in control mice and animals subjected to UUO surgery for 3 d, 7 d or 14 d ($n=3$). **d** Relative transcript levels of genes related to iron metabolism during ferroptosis (GPX4, FPN, DMT1, TFRC, SLC7A11, and SLC3A2) in 3d, 7d and 14d UUO mice. For all panels, the data are presented as the means ± SEMs. For all panels, the data are presented as the means ± SDs. $^*P<0.05$, $^{**}P<0.005$, $^{***}P<0.001$, $^{****}P<0.0001$. ns represents no significance. Statistical analysis was performed via two-way analysis of variance (ANOVA) with the Bonferroni post hoc correction

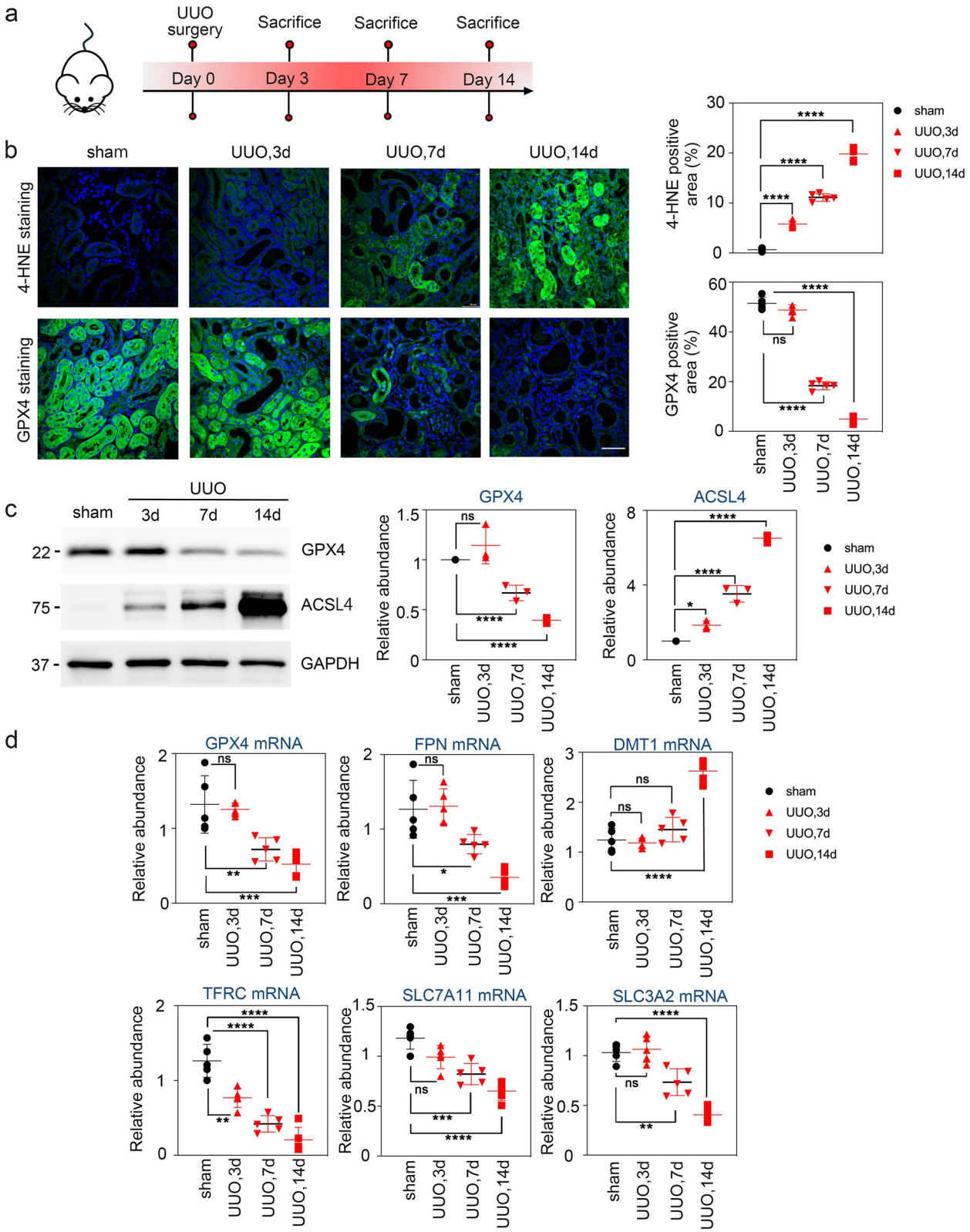

Fig. 1 (See legend on previous page.)

(4-HNE) and the antioxidant protein GPX4. As shown in Fig. 1b, TECs from sham-operated mice expressed high-intensity GPX4 but not 4-HNE. In the UUO 3-day group, 4-HNE was mildly upregulated, with GPX4 remaining steady in the proximal tubule. From day 7 to 14, there was a sharp increase in 4-HNE and a concurrent decrease in GPX4 expression in the obstructed kidney, consistent with protein and mRNA expression of GPX4 (Fig. 1c and d). Ferroptosis sensitivity is affected by lipid metabolism and iron homeostasis. To systematically explore the mechanisms underlying ferroptosis in renal fibrosis, we tested the core lipid metabolic enzymes and iron metabolism-related genes at different time points following UUO. Western blot analysis revealed a time-dependent increase in acyl-CoA synthetase long-chain family member 4 (ACSL4) protein levels starting on day 3. Quantitative PCR analysis of iron homeostasis genes (SLC7A11, SLC3A2, FPN, DMT1, and TFRC) showed slight changes at 3 days post-UUO, followed by a progressive decline at later time points (Fig. 1d). However, the change in the iron metabolic gene was not obvious at an earlier time point, similar to GPX4, which sharply changed at UUO 7 and 14 days. These results suggest that GPX4 is essential for maintaining normal metabolic activity during ferroptosis in mice. The progressive downregulation of GPX4, combined with lipid metabolic enzyme dysfunction, exacerbates lipid peroxidation and iron imbalance, driving the progression of renal interstitial fibrosis.

Pharmacological inhibition of ferroptosis suppresses renal fibrosis induced by UUO

To determine whether target-mediated inhibition of ferroptosis can effectively delay renal fibrosis, we examined the effects of Fer-1, a specific ferroptosis inhibitor that inhibits lipid peroxidation synthesis by reducing oxygen radical production (Fig. 2a) [20, 21]. As shown by the immunofluorescence results in Sup. 1a and Sup. 1c, in kidney tissues, UUO induced accelerated degradation of GPX4, accumulation of 4-HNE and TUNEL-positive cells. By blocking lipid peroxidation, Fer-1 significantly prevented lipid oxidant accumulation and cell death at 14 days post-UUO, as detected by the immunofluorescence of 4-HNE and TUNEL assays (Sup. 1a and Sup. 1c). Additionally, Fer-1 reduced the expression of lipid metabolic enzymes, including ACSL4 and lysophosphatidylcholine acyltransferase 3 (LPCAT3) (Sup. 1b) while elevating the expression of the antioxidation protein GPX4 (Sup. 1a and Sup. 1b). These results indicate that the inhibition of lipid peroxidation by ferroptosis is effective in preventing UUO-induced TEC ferroptosis. To elucidate the role of ferroptosis in regulating renal interstitial fibrosis, we further examined the progression of renal interstitial fibrosis in vivo. UUO kidneys presented severe morphological lesions characterized by tubular dilation, tubulointerstitial expansion, and interstitial collagen deposition. Conversely, the kidneys treated with Fer-1 presented considerably fewer morphological abnormalities (Fig. 2b). Immunofluorescence analysis using fibronectin and α-SMA antibodies revealed that fibronectin and α-SMA expression levels were obviously reduced in UUO mice treated with fer-1 compared to UUO mice (Fig. 2c). The mRNA and protein levels of fibrosis markers (fibronectin, collagen-1, and α-SMA) were consistent with the immunofluorescence results (Fig. 2d and e). In conclusion, pharmacologically effective control of ferroptosis can alleviate the process of renal fibrosis and demonstrate that persistently activated ferroptosis in TECs facilitates the progression of renal fibrosis.

Pharmacological inhibition of TEC ferroptosis attenuates TGF-β/Smad signaling activation in UUO-induced renal fibrosis

Notably, several profibrotic cytokines produced by TECs, such as TGF-β, CTGF, PDGFB, and FGF2, are key regulators of kidney fibrosis development [22, 23]. To explore whether TECs ferroptosis exacerbates renal fibrosis through these profibrotic factors, we examined their expression in obstructed kidneys treated with Fer-1. Under these conditions, the levels of TGF-β and its key downstream effectors (p-Smad2, p-Smad3, CTGF, PDGFB, and FGF2) were notably attenuated. As expected, the protein levels of TGF-β, p-Smad2, and p-Smad3 decreased after Fer-1 treatment in UUO mice, indicating the inhibition of TGF-β/Smad signaling (Fig. 3a). Moreover, Fer-1 treatment significantly reduced the release of profibrotic cytokines, including TGF-β,

(See figure on next page.)

Fig. 2 Pharmacological inhibition of ferroptosis protects against renal fibrosis in UUO mice. **a** C57BL/6 mice were pretreated with the ferroptosis inhibitor Fer-1 (1 mg/kg) for 1 h followed by UUO surgery and then euthanized at 7 d or 14 d. **b** Fer-1 decreased histologic injury in kidneys from UUO-treated mice for 7 and 14 days. Representative images ($n=6$) of Sirius red (scale bars, 1000 μm).), H&E- and Masson trichrome-stained kidney tissue. Scale bars, 50 μm. Morphology was examined via light microscopy. **c** Representative images ($n=5$) of immunofluorescence analysis of fibrosis-associated markers (fibronectin, α-SMA) in mouse kidney sections. Scale bars, 50 μm. **d** Immunoblot analysis of the expression of fibronectin, collagen-1, and α-SMA. **e** Relative transcript levels of genes related to fibrosis in UUO mice after Fer-1 treatment. For all panels, the data represent the mean ± SEM. *$P<0.05$, **$P<0.005$, ***$P<0.001$, ****$P<0.0001$, ns indicates no significance. Statistical analysis was performed via two-way analysis of variance (ANOVA) with the Bonferroni post hoc correction

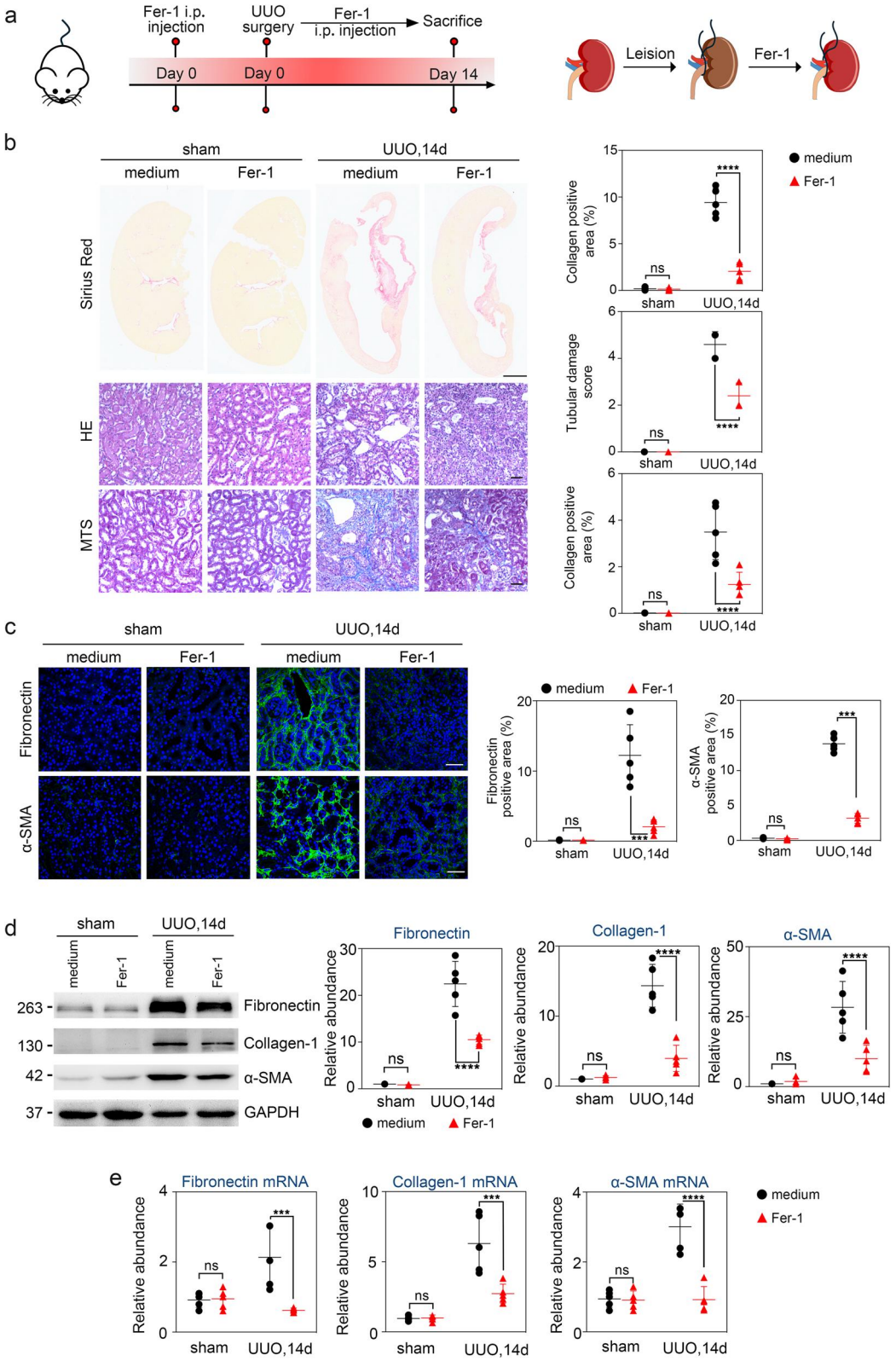

Fig. 2 (See legend on previous page.)

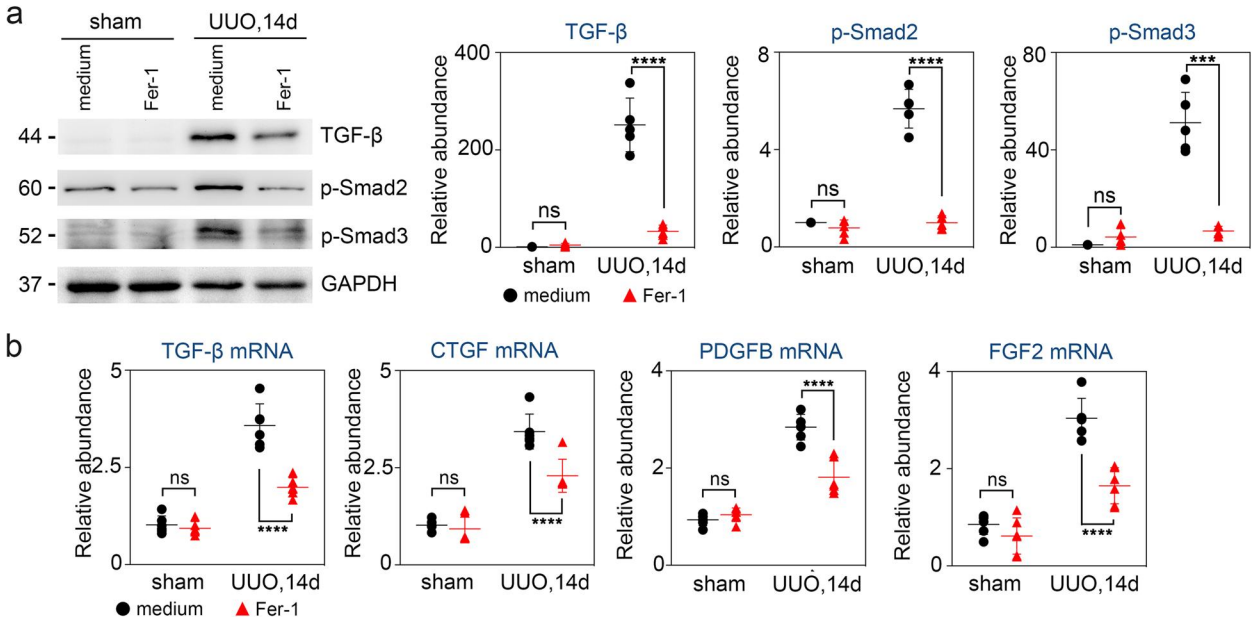

Fig. 3 TGF-β/Smad signaling activation during UUO is attenuated by inhibiting TECs ferroptosis with Fer-1. **a** Western blot analysis of the expression of TGF-β, p-Smad2, and p-Smad3. **b** Relative transcript levels of genes related to profibrotic cytokines (TGF-β, CTGF, PDGFB, and FGF2) in UUO mice after Fer-1 treatment. For all panels, the data are presented as the means ± SDs. *$P < 0.05$, **$P < 0.005$, ***$P < 0.001$, ****$P < 0.0001$, ns indicates no significance. Statistical analysis was performed via two-way analysis of variance (ANOVA) with the Bonferroni post hoc correction

CTGF, PDGFB, and FGF2, from TECs (Fig. 3b). These data indicate that Fer-1 attenuates renal interstitial fibrosis by suppressing TGF-β/Smad signaling and decreasing the production of profibrotic cytokines. Mechanistically, TEC ferroptosis may accelerate renal interstitial fibrosis by activating the TGF-β/Smad signaling pathway and enhancing profibrotic cytokines.

Pharmacological inhibition of ferroptosis alleviates fibrotic changes in TGF-β-treated HK-2 cells

In the present study, TGF-β was identified as an inducer of fibrotic changes and effectively stimulated fibrosis in the HK-2 cells, paralleling the fibrotic processes observed in the UUO mouse model in vivo [24]. Although we demonstrated that Fer-1 improved UUO-induced kidney fibrosis, it is unclear whether Fer-1 might ameliorate TGF-β-induced fibrosis in HK-2 cells. As shown in Fig. 4a, we first examined the occurrence of ferroptosis in HK-2 cells treated with 20 ng/ml TGF-β for 48 h in the absence or presence of Fer-1. As shown in Sup. 2a, b and f, TGF-β effectively activated the accumulation of lipid hydroperoxides, such as 4-HNE, C11-BODIPY oxidation, and MDA. Immunoblotting and quantitative analysis (Sup. 2a and 2b) confirmed that Fer-1 treatment significantly rescued GPX4 protein expression but markedly downregulated ACSL4 and LPCAT3 protein expression (Sup. 2c). Fer-1 treatment restored cell function and reduced damage in the TGF-β-induced HK-2 cells, as measured by the effects of proliferation on cell viability (MTT assay) and cell death (LDH cytotoxicity assay) (Sup. 2d, e). The above results demonstrate that TGF-β induces ferroptosis accumulation, which Fer-1 effectively ameliorates in HK-2 cells.

To further explore the relationship between ferroptosis and renal fibrosis in vitro, we detected fibrotic markers (fibronectin, α-SMA and collagen-1) in TGF-β-induced

(See figure on next page.)

Fig. 4 Pharmacological inhibition alleviates fibrotic changes in HK-2 cells through the TGF-β/Smad signaling pathway in vitro. **a** HK-2 cells treated with 20 ng/ml TGF-β for 48 h in the absence or presence of Fer-1. **b** Representative images of fibronectin and α-SMA immunostaining in HK-2 cells. Scale bars, 50 μm. **c** The protein levels of fibrosis markers (fibronectin, collagen-1, and α-SMA) were detected by immunoblotting. **d** The mRNA levels of fibrosis markers (fibronectin, collagen-1, and α-SMA) were detected via RT–qPCR. **e** Western blot analysis of the expression of TGF-β, p-Smad2, and p-Smad3. **f** Relative transcript levels of genes related to profibrotic cytokines (TGF-β, CTGF, PDGFB, and FGF2) in TGF-β-induced HK-2 cells after Fer-1 treatment. All the data are presented as the means ± SDs from $n = 3$ biological replicates. *$P < 0.05$, **$P < 0.01$, ***$P < 0.001$, ****$P < 0.0001$,. ns represents no significance. Statistical analysis was performed via two-way analysis of variance (ANOVA) with the Bonferroni post hoc correction

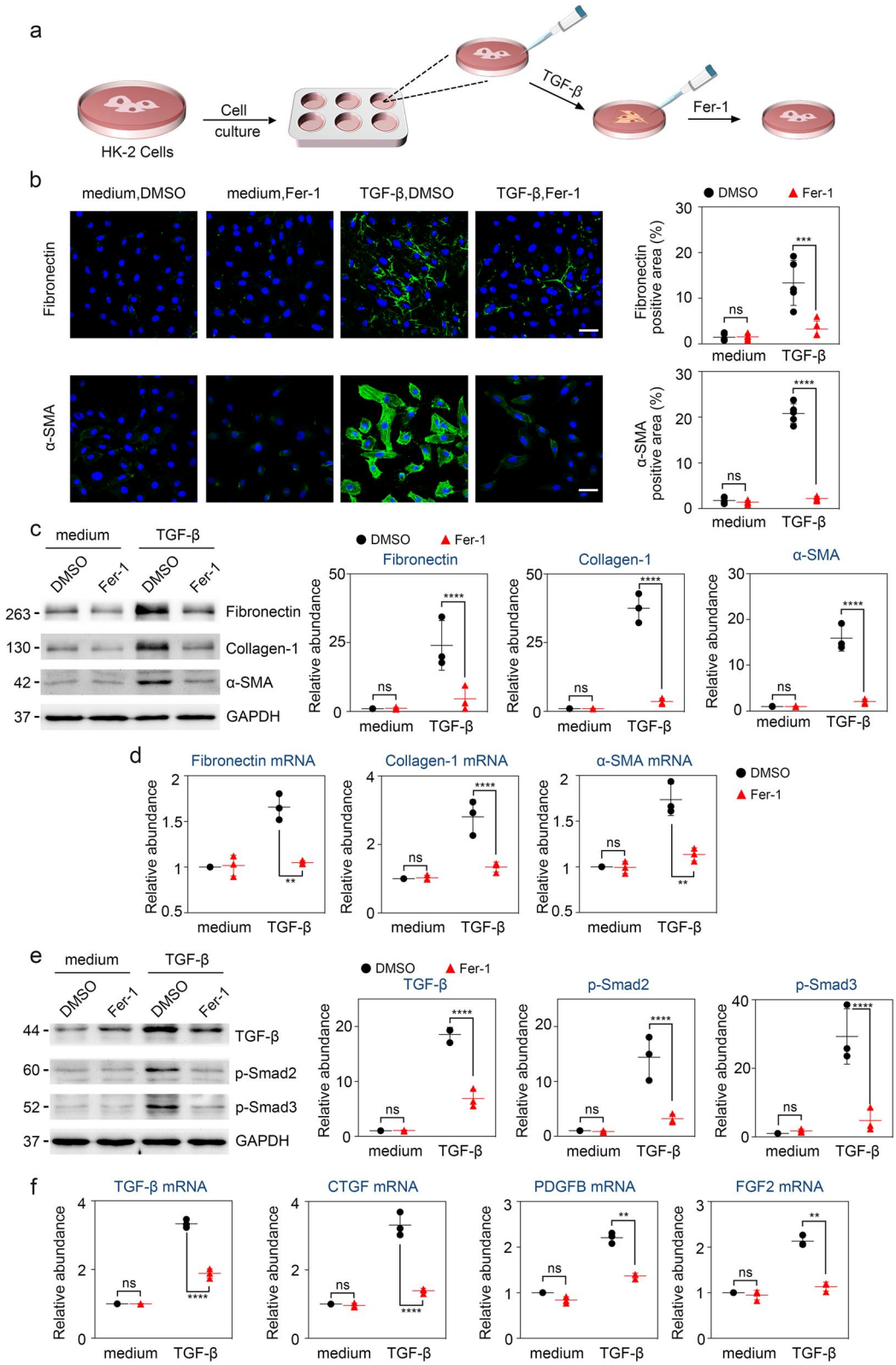

Fig. 4 (See legend on previous page.)

HK-2 cells. As expected, TGF-β-induced accumulation of green fluorescence with fibronectin and α-SMA in HK-2 cells was significantly decreased by Fer-1, as detected by immunofluorescence staining (Fig. 4b). As described above, TGF-β-induced HK-2 cells are accompanied by ferroptosis activation, and HK-2 cells treated with TGF-β also presented increased protein and mRNA levels of fibronectin, collagen-1, and α-SMA. After Fer-1 administration to HK-2 cells for 48 h, the expression of fibrotic factors decreased (Fig. 4c, d). These results suggest that TGF-β-induced fibrosis in HK-2 cells is effectively rescued by inhibiting ferroptosis. Persistent activation of ferroptosis aggravated fibrosis in the TGF-β-treated HK-2 cells.

Ferroptosis inhibition attenuates the TGF-β-induced profibrotic reaction through TGF-β/Smad signaling in vitro

In addition to inducing ferroptosis activation, TGF-β also promotes fibrotic changes in HK-2 cells [25]. To further determine the mechanism by which ferroptosis triggers fibrotic reactions in vitro, we examined changes in the levels of the profibrotic factors, including components of the TGF-β/Smad signaling pathway and profibrotic cytokines. Consistently, TGF-β induced high expression of TGF-β, p-Smad2, and p-Smad3 and profibrotic cytokines (TGF-β, CTGF, PDGFB, and FGF2), which was also suppressed by the ferroptosis inhibitor Fer-1 (Fig. 4e and f). These data suggest that ferroptosis plays a critical role in renal fibrosis by sustaining the activation of TGF-β/Smad signaling and promoting the release of downstream profibrotic factors, ultimately contributing to fibrogenesis.

Ferroptosis in TECs is repaired in GPX4-overexpressing mice during UUO

The findings of pharmacological experiments effectively illustrated that inhibiting TEC ferroptosis can rescue renal fibrosis through TGF-β/Smad signaling. To further define the role of TEC ferroptosis in renal interstitial fibrosis, we employed adeno-associated viral vectors to overexpress GPX4 (AAV9-mGPX4) or deliver a control vector (AAV9-Vector) to renal proximal TECs (Fig. 5a). First, we tested the efficacy of GPX4 overexpression in mouse kidney tissue. As shown in Sup. 3a and 3b, we found that GPX4 was effectively overexpressed in the sham group following AAV-GPX4 injection. Using AAV-GPX4-injected mice, we detected the effectiveness of ferroptosis inhibition in UUO for 14 days. Fourteen days after UUO, the AAV-Ctrl-injected mice presented decreased GPX4 expression and accumulation of lipid hydroperoxide (4-HNE)- and TUNEL-positive cells, as detected by immunofluorescence and TUNEL assays (Sup. 3a and 3c). However, the conversion of GPX4 and 4-HNE and cell death were strikingly inhibited in the GPX4-overexpressing mice. Moreover, we detected lipid metabolism enzymes, such as ACSL4 and LPCAT3, which were effectively reduced in GPX4-OE mice (Sup. 3b). Compared with that in the kidney tissues of the AAV-Ctrl-injected mice, GPX4 expression was largely increased in the kidney tissues of both the sham and UUO groups. Consistently, the overexpression of GPX4 in TECs effectively reversed the exacerbation of ferroptosis progression.

Ferroptosis deficiency in GPX4-overexpressing mice protects against renal interstitial fibrosis during UUO

Using GPX4-overexpressing (GPX4-OE) mice, we investigated the role of TEC ferroptosis in the progression of renal interstitial fibrosis. In UUO-induced kidneys, severe morphologic lesions, including tubular dilation, tubulointerstitial expansion, and interstitial collagen deposition, were observed. However, GPX4-OE kidneys presented considerably fewer morphologic abnormalities according to morphometric analyses (Fig. 5b). As shown by immunofluorescence analysis with fibronectin and α-SMA antibodies (Fig. 5c), red fluorescence intensity was induced in UUO-induced kidneys and markedly suppressed in GPX4-OE kidneys. Consistently, the UUO-induced upregulation of fibrosis marker (fibronectin, collagen-1, and α-SMA) protein expression echoed the immunofluorescence results and was attenuated in GPX4-OE mice (Fig. 5d). These observations were verified by mRNA analysis of fibronectin, collagen-1, and α-SMA (Fig. 5e). Consistent with the pharmacological results, the above results provide convincing evidence

(See figure on next page.)

Fig. 5 Ferroptosis deficiency in GPX4-overexpressing mice protects against renal interstitial fibrosis during UUO. **a** Mice were injected with AAV9-mGPX4 or AAV9-vector in renal proximal tubular epithelial cells and then subjected to UUO surgery. **b** Fer-1 decreased histologic injury in kidneys from mice subjected to UUO for 7 and 14 days. Representative images ($n=6$) of Sirius red (scale bars, 1000 μm).), H&E- and Masson trichrome-stained kidney tissue. Scale bars, 50 μm. Morphology was examined via light microscopy. **c** Representative images ($n=5$) of immunofluorescence analysis of fibrosis-associated markers (fibronectin, α-SMA) in mouse kidney sections. Scale bars, 50 μm. **d** Immunoblot analysis of the expression of fibronectin, collagen-1, and α-SMA. **e** Relative transcript levels of genes related to fibrosis in UUO mice after Fer-1 treatment. For all panels, the data are presented as the means ± SDs. *$P<0.05$, **$P<0.005$, ***$P<0.001$, ****$P<0.0001$, ns indicates no significance. Statistical analysis was performed via two-way analysis of variance (ANOVA) with the Bonferroni post hoc correction

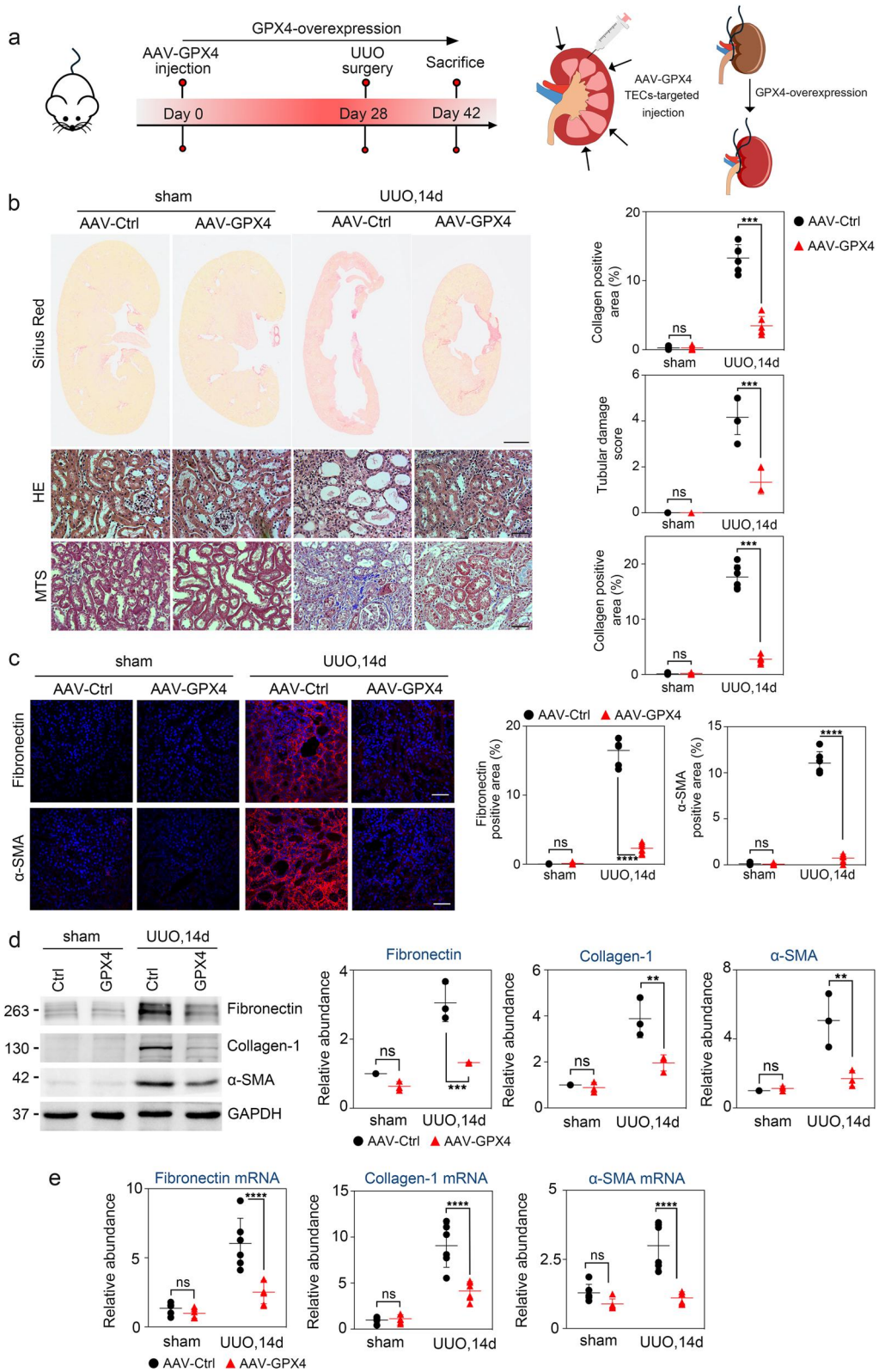

Fig. 5 (See legend on previous page.)

that the GPX4 overexpression protects TECs from ferroptosis and mitigates renal interstitial fibrosis.

Ferroptosis deficiency protects the kidney from fibrotic changes through TGF-β/Smad signaling

In addition to the fibrosis that is induced by ferroptosis during UUO, we also explored TGF-β/Smad signaling and the production of profibrotic cytokines (TGF-β, CTGF, PDGFB, and FGF2) by TECs. Alongside pharmacological findings, our data indicate that ferroptosis defects caused by GPX4 overexpression significantly prevent the progression of fibrosis by blocking the expression of cytokines. As shown in Fig. 6a, GPX4 overexpression reduced the UUO-induced upregulation of TGF-β, p-Smad2, and p-Smad3. Additionally, the activity of profibrotic cytokines was significantly decreased in GPX4-OE kidney tissues (Fig. 6b). Together, these results, in alignment with in vivo and in vitro findings using Fer-1, demonstrate that inhibiting TEC ferroptosis protects against renal interstitial fibrosis through the inhibition of TGF-β/Smad signaling.

Ferroptosis activation in TGF-β-treated HK-2 cells is suppressed by GPX4 overexpression

Our in vivo studies revealed the role of GPX4 overexpression in attenuating TEC ferroptosis and fibrotic changes during UUO. To further explore the relationship between ferroptosis and fibrotic factors in HK-2 cells, we established a GPX4-overexpressing plasmid system in HK-2 cells and treated the cells with TGF-β for 48 h (Fig. 7a). TGF-β-induced HK-2 cells exhibited increased ferroptotic sensitivity, as detected by high levels of lipid peroxidation (Sup. 4a and 4b), which were confirmed through immunofluorescence analysis of C11 BODIPY 581/591

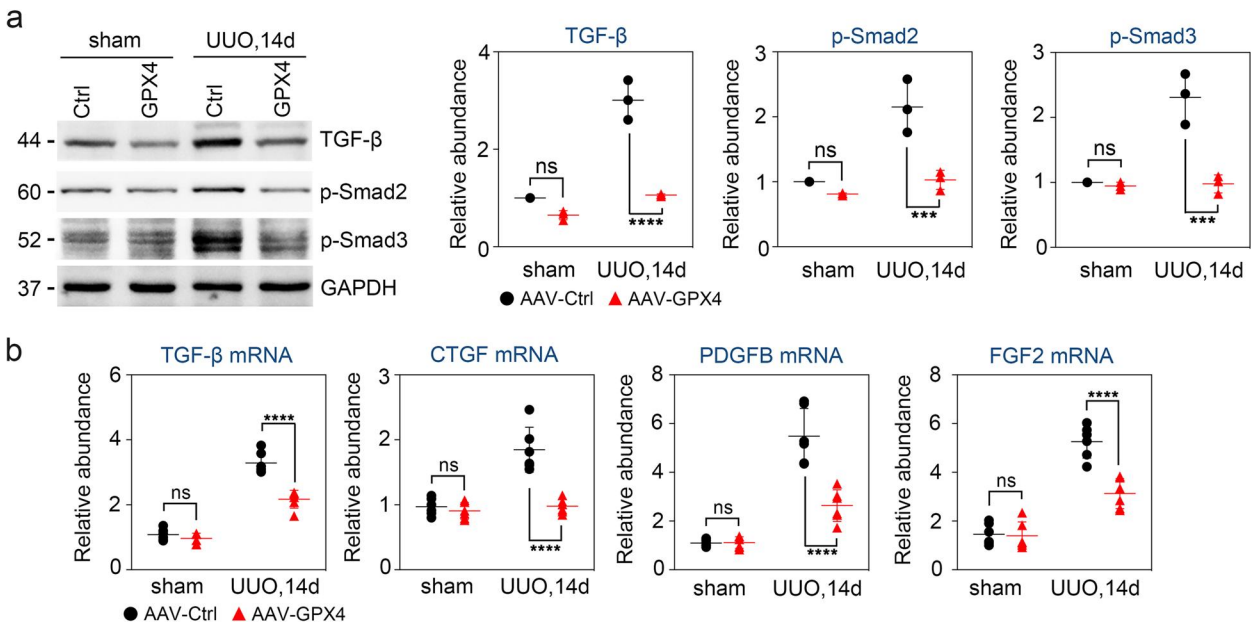

Fig. 6 TGF-β/Smad signaling activation during UUO is inhibited by ferroptosis deficiency in GPX4-overexpressing mice. **a** Western blot analysis of the expression of TGF-β, p-Smad2, and p-Smad3. **b** Relative transcript levels of genes related to profibrotic cytokines (TGF-β, CTGF, PDGFB, and FGF2) in UUO mice overexpressing GPX4. For all panels, the data are presented as the means ± SDs. *$P < 0.05$, **$P < 0.005$, ***$P < 0.001$, ****$P < 0.0001$, ns indicates no significance. Statistical analysis was performed via two-way analysis of variance (ANOVA) with the Bonferroni post hoc correction

(See figure on next page.)

Fig. 7 Upregulation of GPX4 in HK-2 cells attenuates fibrotic changes by activating TGF-β/Smad signaling. **a** Control and GPX4 overexpression plasmid systems were established separately, and HK-2 cells were cultured with TGF-β for 48 h. **b** Representative images of fibronectin and α-SMA immunostaining in HK-2 cells. Scale bars, 25 μm. **b** The protein levels of fibrosis markers (fibronectin, collagen-1, and α-SMA) were detected by immunoblotting. **c** The mRNA levels of fibrosis markers (fibronectin, collagen-1, and α-SMA) were detected via RT–qPCR. **d** Western blot analysis of the expression of TGF-β, p-Smad2, and p-Smad3. **e** Relative transcript levels of genes related to profibrotic cytokines (TGF-β, CTGF, PDGFB, and FGF2) in TGF-β-induced HK-2 cells after Fer-1 treatment. All the data are presented as the means ± SDs from $n = 3$ biological replicates. For all panels, the data are presented as the means ± SDs. *$P < 0.05$, **$P < 0.005$, ***$P < 0.001$, ****$P < 0.0001$, ns indicates no significance. Statistical analysis was performed via two-way analysis of variance (ANOVA) with the Bonferroni post hoc correction

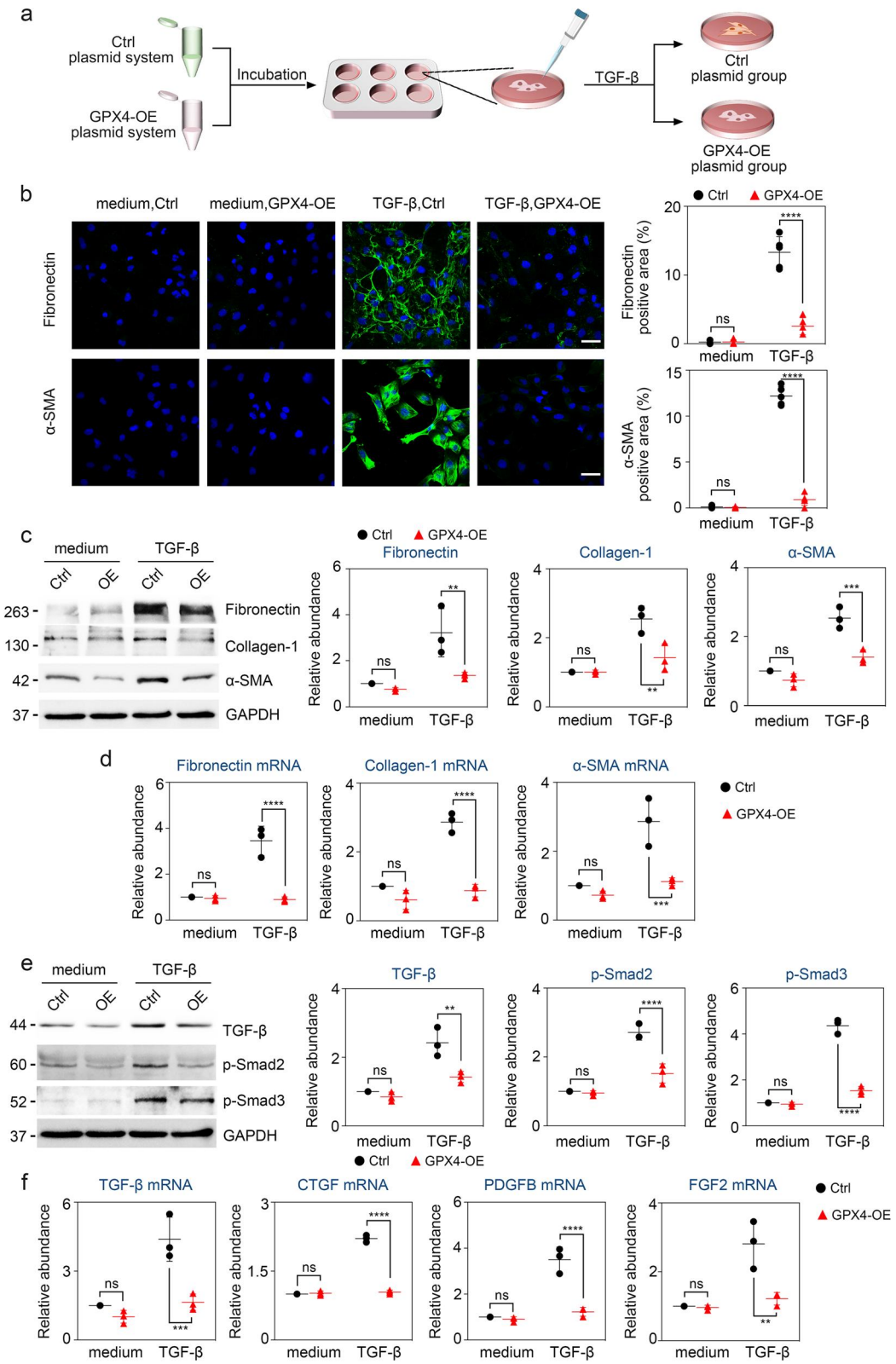

Fig. 7 (See legend on previous page.)

and 4-HNE. Importantly, the addition of the GPX4 plasmid suppressed TGF-β-induced ferroptosis in HK-2 cells. We next examined the protein expression of key lipid metabolic enzymes involved in ferroptosis (GPX4, ACSL4 and LPCAT3). Consistent with the immunofression significantly alleviated the lipid metabolic enzymes that aggravated lipid hydroperoxide (Sup. 4c). Together with the pharmacological findings, the effects of TGF-β-induced cell function and damage in HK-2 cells were measured via the effects of proliferatin on cell viability (MTT assay) and cell death (LDH cytotoxicity assay), and both effects were reversed by GPX4 overexpression (Sup. 4d and 4e). Furthermore, we detected the content of malondialdehyde (MDA), a marker of lipid peroxidation, and found that TGF-β treatment increased MDA content, which was mitigated in GPX4-OE cells (Sup. 4f). These results further demonstrate that the accumulation of TGF-β-induced ferroptosis was effectively ameliorated by GPX4 overexpression.

Ferroptosis deficiency attenuated TGF-β-induced fibrosis in HK-2 cells via GPX4 overexpression

These results demonstrated that ferroptosis inhibition improved fibrotic changes in vitro and in vivo. It is not clear whether ferroptosis deficiency combined with GPX4 overexpression might ameliorate TGF-β-induced fibrosis in HK-2 cells. We first examined the expression of fibrotic markers (fibronectin and α-SMA) via immunofluorescence staining, which revealed low green fluorescence intensity in the TGF-β-induced group after GPX4 overexpression (Fig. 7b). We subsequently detected protein expression and mRNA expression of fibronectin, collagen-1, and α-SMA. As shown in Fig. 7c and d, GPX4 overexpression in TGF-β-treated HK-2 cells was also characterized by reduced protein and mRNA expression. Notably, both Fer-1 treatment and GPX4 overexpression mitigated TGF-β-induced ferroptosis in renal interstitial fibrosis. The inhibition of ferroptosis effectively reduced damage to TECs during fibrosis, as confirmed in GPX4-OE HK-2 cells. These results further demonstrate that ferroptosis deficiency alleviated the fibrotic changes in TGF-β-treated HK-2 cells.

TGF-β/Smad signaling activation during HK-2 is attenuated by inhibiting ferroptosis with GPX4 overexpression

According to the above experimental results, it is worth investigating whether ferroptosis deficiency attenuates fibrosis through TGF-β/Smad signaling in TGF-β-treated HK-2 cells. Ferroptosis-induced profibrotic progression was largely inhibited in GPX4-overexpressing cells, as indicated by immunoblot analysis (TGF-β, p-Smad2, and p-Smad3) (Fig. 7e). Furthermore, we examined the effects of GPX4 overexpression on the mRNA expression of profibrotic cytokines (TGF-β, CTGF, PDGFB, and FGF2). As shown in Fig. 7f, TGF-β activated the expression of profibrotic cytokines in HK-2 cells, which was completely alleviated in GPX4-OE cells. These findings suggest that GPX4 overexpression leads to ferroptosis deficiency in HK-2 cells and that the progression of TGF-β-induced fibrosis might be regulated by ferroptosis through the TGF-β/Smad signaling pathway and related profibrotic cytokines.

Discussion

The involvement of typical ferroptosis damage, such as altered mitochondrial morphology and iron overload, has been observed in kidney diseases [26–28]. Nevertheless, kidney fibrosis is the end-stage renal disease (ESRD) and always be accompanied by the damage of ferroptosis-susceptible field, which is refered as iron metabolism, oxidative stress, inflammation, and autophagy [29–31]. The TECs is the most vulnerable cells to ferroptosis in CKD. Both iron chelator and antioxidant treatments are effective in reducing TECs iron overload, lipid peroxidation and improving renal fibrosis [11, 13]. There is no doubt that target ferroptosis in TECs to inhibit kidney fibrosis is an effective therapeutic measure. However, the mechanisms of renal fibrosis which is drived by TECs ferroptosis remain need to be elucidated. Therefore, we explored the potential ferroptotic triggers from time dimensions of CKD and uncovered the mechanisms caused by TECs ferroptosis, which is crucial to reduce the cascade effect of ferroptosis and alleviated kidney fibrosis.

In the present study, we found that ferroptosis is a maladaptive process in the progression of renal fibrosis and that the persistent activation of ferroptosis is an accelerator of renal interstitial fibrosis in renal tubular epithelial cells. Inhibiting the accumulation of ferroptosis by pharmacological interaction (Fer-1) and overexpressing GPX4 in TECs effectively alleviated TEC lesions and matrix collagen deposition during UUO. This suppresses the TGF-β/Smad signaling pathway and attenuates the release of profibrotic cytokines by TECs. These results collectively demonstrate that inhibiting TECs ferroptosis is a promising therapeutic target for treating kidney fibrosis and the expression of profibrotic factors.

While the critical role of ferroptosis in TECs in CKD was validated in our previous study [13], the pathological mechanisms by which TECs ferroptosis induces or exacerbates kidney fibrosis remain largely unknown. Ferroptosis is regulated by multiple cellular metabolic events, including redox homeostasis, iron metabolism, and amino acid metabolism [32, 33]. As a complex form of programmed cell death, ferroptosis involves two major driving mechanisms: iron overload and lipid peroxidation [6, 12]. Through ongoing investigations into the

mechanisms of ferroptosis, several proteins have been identified as protective factors that limit lipid peroxidation, including GPX4 [18] and FSP1 [34]. GPX4, in particular, plays a crucial role in ferroptosis by converting harmful lipid peroxides into non-toxic lipid alcohols [18]. The inactivation of GPX4 in cells culminates in phospholipid peroxidation and cell death, which can be mitigated by ferroptosis inhibitors [19]. Selenocysteine utilization by GPX4 confers exquisite resistance to irreversible overoxidation as cells expressing a cysteine variant are highly sensitive to peroxide-induced ferroptosis [35].

Building on these two mechanisms, we explored the relationship between ferroptosis and renal fibrosis. We subsequently simulated different renal fibrosis processes by constructing UUO models at multiple time points. During the initial 3 days of UUO, lipid metabolic enzymes and lipid hydroperoxides, such as ACSL4 and 4-HNE, accumulated in TECs through several pathways. However, genes associated with iron metabolism (e.g., SLC7A11, SLC3A2, FPN, DMT1, and TFRC) and GPX4 remained largely unchanged, maintaining normal homeostasis. Accompanied by the downregulation of GPX4, lipid metabolic enzyme dysfunction further drives the disruption of lipid peroxidation and iron imbalance during the middle and late stages of renal fibrosis, which is consistent with previous report [13, 14, 36, 37].

The above findings revealed that lipid peroxidation is significantly altered during the early stages of renal fibrosis. To further investigate, we targeted lipid peroxidation using pharmacological experiments. Fer-1 is a synthetic radical-trapping antioxidant (RTA) that blocks ferroptosis by reducing the accumulation of lipid hydroperoxides [5, 20]. We found that inhibiting ferroptosis effectively delayed fibrosis progression, suggesting that TECs ferroptosis contributes to renal fibrosis. Given the critical role of GPX4 in ferroptosis, we further explored its involvement in renal fibrosis. Previous studies have reported that GPX4 genetic deficiency leads to nephrotoxic effects [19], and its role in ischemia/reperfusion-induced acute kidney injury and obstructive renal fibrosis is well-documented [14, 38]. In our study, GPX4 expression negatively correlated with fibrosis severity in UUO mice at 7 and 14 days. Furthermore, overexpressing GPX4 in kidney TECs markedly ameliorated renal interstitial fibrosis by counteracting ferroptosis. These findings suggest that maintaining GPX4 activity may be a promising therapeutic strategy for preventing renal fibrosis.

Consistent with our previous study [13], we demonstrated that kidney fibrosis is associated with cell death in TECs, a pathologically relevant form of ferroptosis. Our findings further suggested that TECs ferroptosis contributes to renal fibrosis and may exacerbate its progression. TGF-β is a central mediator of renal fibrosis, and its stimulation has become a widely used in vitro model for studying cellular fibrosis. Interestingly, TGF-β-stimulated TECs exhibited lipid peroxidation similar to that observed in cells treated with the ferroptosis inducer erastin [28]. Moreover, TGF-β suppressed SLC7A11/xCT expression via Smad3 activation and enhanced lipid peroxidation in hepatocellular carcinoma cells [28, 39]. In our study, we developed a cell fibrosis model by stimulating TECs with TGF-β, which resulted in lipid peroxide accumulation in HK-2 cells. Treatment with Fer-1 effectively inhibited ferroptosis and significantly alleviated fibrotic changes in these cells. TECs, key components of the kidney, are vulnerable to physical and chemical damage, including hypoxia, toxins, proteinuria, metabolic diseases, and senescence [4]. Inhibition of ferroptosis alleviated inflammatory cell infiltration and MCP-1 release from TECs [40]. In addition, evidence suggests that ferroptotic stress promotes the accumulation of proinflammatory TECs during maladaptive renal repair. Genetic induction of high ferroptotic stress in TECs after mild injury leads to the accumulation of inflammatory proximal tubular cells, enhancing inflammation and fibrosis [41]. Maladaptive repair of TECs leads to the transformation of injured TECs into a secretory phenotype and elicits proinflammatory (e.g., interleukin, tumor necrosis factor, and chemokine) [42–44]and profibrotic cytokines [45] (e.g., TGF-β and CTGF). One team reported that the occurrence of ferroptosis is closely connected with the profibrotic phenomenon, but further causal connections, which are based on the ferroptosis convolution mechanism, have not been explored [14]. In this study, we demonstrated that ferroptosis acts as a trigger for profibrogenesis, as evidenced by both pharmacological and genetic approaches. Our results showed that inhibiting ferroptosis reduced the release of profibrotic cytokines from TECs and suppressed the TGF-β/Smad signaling pathway during fibrosis. Thus, inhibiting TECs ferroptosis could offer a novel therapeutic strategy for preventing CKD.

Conclusion

TECs ferroptosis is a critical pathological mechanism in renal fibrotic disease, in which ferroptosis exacerbates renal fibrosis. The inhibition of TECs ferroptosis can effectively ameliorate renal interstitial fibrosis and significantly reduce the expression of profibrotic factors through the inhibition of TGF-β/Smad signaling.

Materials and methods

Mice

All animal procedures were in strict compliance with the National Health and Medical Research Council of China. All the animal studies were reviewed and approved by

the animal ethics review board of Tongji Medical College. Eight-week-old male C57BL/6 mice were bred in a specific pathogen-free (SPF) environment in the laboratory animal center of Tongji Medical College. UUO mice were generated as described previously. In brief, the mice were anesthetized with 1% pentobarbital sodium, and the left ureter was isolated and ligated. After surgery, the mice were maintained in a temperature-controlled room with a 12-h light/dark cycle and reared on standard chow water ad libitum. UUO was maintained for 7 or 14 d. Ferrostatin-1 (Fer-1, Sigma–Aldrich, Catalog SML0583, ferroptosis inhibitor; 1 mg/kg/d) was administered 1 h before UUO surgery through intraperitoneal injection, or normal saline, which served as a control. At the time of euthanasia, kidney samples were collected for immunoblotting, qRT–PCR, and immunofluorescence staining.

Cell lines

The human proximal tubular epithelial cell line HK-2 was obtained from the China Centre for Type Culture Collection (CCTCC, China). The cells were cultured in DMEM-F12 (HyClone) supplemented with 10% FBS and 1% penicillin/streptomycin at 37 °C in a humidified atmosphere of 5% CO_2. The chemicals used to treat the cells were as follows: recombinant human TGF-β1 (PeproTech, Catalog 100–21 C-10, 20 ng/mL), erastin (Sigma–Aldrich, Catalog E7781, ferroptosis inducer; 5 μM), and Fer-1 (2 μM). Treated cells were harvested and used for various morphological and biochemical studies. Additional gene transfection studies included the use of a GPX4 plasmid (origene, catalog RC208065; 5 μg) in cells transfected with Lipofectamine 3000 (Thermo Fisher Scientific, MA).

Renal histopathology

Mouse kidney samples were fixed in 4% paraformaldehyde overnight and embedded in paraffin. Five-micron-thick paraffin sections were subjected to hematoxylin–eosin (HE), periodic acid–Schiff (PAS), and Masson's trichrome (MTS) staining. The tubular injury score was evaluated on the basis of the following morphologic changes, including necrotic tubules, loss of brush borders, tubule dilation, cast formation, tubular epithelial swelling, and vacuolar degeneration: 0, no morphologic deformities; 1, <10%; 2, 10-25%; 3, 25-50%; 4, 50-75%; and 5, ≥75%. The morphology of the tubules in the tissue sections was evaluated via optical microscopy (Mshot, China).

Adenovirus delivery in proximal tubular cells

To achieve the overexpression of GPX4 in proximal tubular cells, AAV9-mGPX4 or AAV9-vector at a dosage of 2.0×10^{10} pfu was delivered into the mouse kidney (8-week-old C57BL/6 mice) by intraparenchymal injection 14 days before the UUO model was established. Adenoviruses were obtained from Vigenebio (Shandong, China).

Gene transfection

pCMV6-GPX4 and pCMV6-Entry plasmids were obtained from OriGene (catalog numbers RC208065 and PS100001). Before transfection, the cells were directly seeded onto 6-well or 96-well plates and grown to a confluence of 40-50%. Lipofectamine 3000 (Thermo Fisher, MA) was used according to the manufacturer's instructions. HK-2 cells were transfected with 5 μg of DNA and incubated for 24 h before use.

MTT assay

HK-2 cells were seeded onto 96-well plates (~3000 cells per well). The cells were treated with 20 ng/ml TGF-β1 for 48 h. The growth medium was removed after treatment, and the cells were cultured in 1x MTT (Keygen Biotech, catalog KGA311) in fresh growth medium for 4 h. Supernatants were carefully removed from the wells. Then, 150 μL of DMSO was added to each well. The 96-well plates were subjected to orbital shaking for 10 min to completely dissolve the formazan. The absorbance at 490 nm was measured with a microplate reader.

Lactate dehydrogenase (LDH) assay

Cell death was measured via a lactate dehydrogenase (LDH, Roche, catalog 04744926001) assay according to the manufacturer's instructions. OD values were measured at 492 nm and referenced at 620 nm by a microplate photometer.

Lipid peroxidation measurement

The cells were seeded on 6-well plates and incubated overnight. The next day, the cells were treated with the test compounds for the indicated times and then incubated with C11-BODIPY 581/591 (Thermo Fisher, catalog D3861) at a working concentration of 5 μM for 30 min at 37 °C. Images were acquired under a confocal microscope (Nikon C2, Japan).

MDA assay

The quantification of malondialdehyde (MDA) levels in HK-2 cells was performed with a lipid peroxidation MDA assay kit (Jiancheng, Nanjing, catalog A003-1) according to the manufacturer's instructions. The MDA content was detected at 450 nm. The MDA concentration was normalized to the total protein concentration.

Immunofluorescence staining

Mouse kidney biopsy paraffin sections were deparaffinized with xylene and ethanol to ablate peroxidase activity, and a pressure cooker was used. After being blocked with 5% BSA for 1 h, the sections were incubated with primary antibodies overnight at 4 °C. The next day, kidney sections were incubated with secondary antibodies for 1 h.

HK-2 cells that had undergone various treatments were fixed in 4% paraformaldehyde. After being blocked with 10% goat serum at room temperature for 1 h, the cells were incubated with primary antibodies overnight at 4 °C. After washing, the cells were incubated with secondary antibodies for 1 h and then washed and mounted.

Images were acquired via confocal microscopy. The raw imaging data were processed via Nikon Software, ImageJ, and Adobe Photoshop. (Nikon C2, Japan).

The primary antibodies used were anti-4-HNE (Abcam, catalog ab4654, 1:100), anti-GPX4 (Abcam, catalog ab125066, 1:200), anti-fibronectin (Abcam, catalog ab45688, 1:100), and anti-α-SMA (Abcam, catalog ab124964, 1:100).

Quantitative PCR with reverse transcription

Total RNA was extracted from cells and mouse kidneys via a HiPure Total RNA Mini Kit (R4111–03, Magen, China) following the manufacturer's instructions. cDNA was synthesized via the ReverTra Ace qPCR RT Kit (FSQ-101; Toyobo, Japan). The quantitative PCR mixtures were prepared with SYBR Green PCR Mix (QPK-201, Toyobo, Japan). PCRs were performed and analyzed on an ABI Step One Plus system (Applied Biosystems, USA); a list of the primers used is provided in Table 1 Sequences of primers.

TUNEL staining of renal tissues

Mouse kidney biopsy paraffin sections were deparaffinized with xylene and ethanol to ablate peroxidase activity and stained with a TUNEL kit (A113, Vazyme, China) following the protocol of the product instructions. The stained sections were observed via confocal microscopy (Nikon C2, Japan). The average number of TUNEL-positive cells in 6 fields of each section was counted, and the ratio of cell death was calculated.

Immunoblotting

Kidney tissues and cells were lysed in RIPA lysis buffer containing a protease inhibitor cocktail and then

Table 1 Sequences of primers

Human Gene	Forward (5′→3′)	Reverse (5′→3′)
Fibronectin	AATAGATGCAACGATCAGGACA	GCAGGTTTCCTCGATTATCCTT
Collagen-1	CCACCAATCACCTGCGTACA	CATCGCACAACACCTTGCC
α-SMA	CTCTGGACGCACAACTGGCATC	GGCATGGGGCAAGGCATAGC
TGF-β	CTGTACATTGACTTCCGCAAG	TGTCCAGGCTCCAAATGTAG
FGF2	CATCAAGCTACAACTTCAAGCA	CCGTAACACATTTAGAAGCCAG
PDGFB	GATCCGCTCCTTTGATGATCTC	GGTCATGTTCAGGTCCAACTC
CTGF	ATTCTGTGGAGTATGTACCGAC	GTCTCCGTACATCTTCCTGTAG
GAPDH	ACCAAATCCGTTGACTCCGAC	CTCCTGTTCGACAGTCAGCC
Mouse Gene	Forward (5′→3′)	Reverse (5′→3′)
Fibronectin	ACAGTCCAGCAAGCAGCAAGC	TGGTGGTCACTCTGTAGCCTGTC
Collagen-1	GGCAAAGATGGAGAAGCTGG	GGAAACCTCTCTCGCCTCTT
α-SMA	GGCTTCGCTGGTGATGATGCTC	TCCCTCTCTTGCTCTGGGCTTC
TGF-β	CCAGATCCTGTCCAAACTAAGG	CTCTTTAGCATAGTAGTCCGCT
FGF2	AGTTGTGTCTATCAAGGGAGTG	CATTGGAAGAAACAGTATGGCC
PDGFB	GTCCAGGTGAGAAAGATTGAGA	GTCATGGGTGTGCTTAAACTTT
CTGF	AAAGCAGCTGCAAATACCAATG	AAATGTGTCTTCCAGTCGGTAG
GPX4	ATAAGAACGGCTGCGTGGTGAAG	TAGAGATAGCACGGCAGGTCCTTC
TFRC	GTGGAGTATCACTTCCTGTCGC	CCCCAGAAGATATGTCGGAAAGG
FPN	GGGTGGATAAGAATGCCAGAC	CCTTTGGATTGTGATCGCAGT
DMT1	CAATGTCTTTGTCGTGTCCGT	GCGACCATTTTAGGTTCAGGAAT
Slc3a2	TTCCTCACCTGACCTCTTCTCCTAC	CTCGGAAGTTGAGCACCACCAG
Slc7a11	GGCACCGTCATCGGATCAG	CTCCACAGGCAGACCAGAAAA
β-actin	GTGCTATGTTGCTCTAGACTTCG	ATGCCACAGGATTCCATACC

centrifuged, after which the supernatants were collected. After protein concentrations were detected with a BCA protein assay kit (Boster, catalog AR0146), 5x SDS was added. The lysates were subjected to electrophoresis, separated on 8–12% polyacrylamide gels and then transferred to PVDF membranes. The membranes were blocked for 1 h in 5% skim milk and incubated overnight at 4 °C with primary antibodies. After washing, the membranes were incubated for 1 h with horseradish peroxidase-labeled secondary antibodies. The bands were visualized via chemiluminescence. Immunoblotting was performed with the following primary antibodies: anti-GPX4 (Abcam, catalog ab125066, 1:3000), anti-ACSL4 (Santa Cruz, catalog sc-365230, 1:1000), anti-LPCAT3 (Abcam, catalog ab232958, 1:500), anti-fibronectin (Abcam, catalog ab45688, 1:5000), anti-collagen-I (Proteintech, catalog 14695-1-AP, 1:1000), and anti-α-SMA (Abcam, catalog ab124964, 1:2000).

Statistics and reproducibility

The data are presented as the means ± SDs. Statistical significance was assessed via two-tailed Student's *t* test or two-way analysis of variance (ANOVA) with the Bonferroni post hoc correction via GraphPad Prism 8.0 (GraphPad). P values < 0.05 were considered statistically significant. The number of samples for each group was chosen on the basis of the expected levels of variation and consistency. All experiments were independently repeated at least three times with similar results.

Abbreviations

CKD	Chronic kidney disease
TECs	Tubular epithelial cells
UUO	Unilateral ureteral obstruction
IRI	Including ischemia-reperfusion injury
Fer-1	Ferrostatin-1
GPX4	Glutathione peroxidase 4
ACSL4	Acyl-CoA synthetase long-chain family 4
LPCAT3	Lysophosphatidylcholine acyltransferase 3
TFRC	Transferrin receptor protein 1
DMT1	Divalent metal transporter 1
FPN	Ferroportin
CTGF	Connective tissue growth factor
PDGFB	Platelet-derived growth factor subunit b
FGF2	Fibroblast growth factor 2
4-HNE	4-hydroxynonenal
MDA	Malondialdehyde

Supplementary Information

The online version contains supplementary material available at https://doi.org/10.1186/s12964-025-02068-4.

Supplementary Material 1: Supplementary Figure 1. Fer-1 attenuates ferroptosis in TECs from UUO mice. a, Representative images ($n = 5$) of 4-HNE-treated mouse kidney sections. Scale bars, 50 μm. b, Immunoblot analysis of the expression of GPX4, ACSL4, and LPCAT3 ($n = 3$). For all panels, the data are presented as the means ± SDs. c, Representative images ($n = 5$) of renal sections subjected to TUNEL staining of the mouse kidney on day 14 with Fer-1. Scale bars, 50 μm. For all panels, the data are presented as the means ± SDs. *$P < 0.05$, **$P < 0.005$, ***$P < 0.001$, ****$P < 0.0001$, ns indicates no significance. Statistical analysis was performed via two-way analysis of variance (ANOVA) with the Bonferroni post hoc correction.

Supplementary Material 2: Supplementary Figure 2. Fer-1 attenuated TGF-β-induced ferroptosis in HK-2 cells. a, Representative images of 4-HNE immunostaining in HK-2 cells. Scale bars, 50 μm. b, Lipid peroxidation was detected via BODIPY 581/591 C11 staining via confocal microscopy. Scale bars, 25 μm. c, Protein expression (western blot) of GPX4, ACLS4, and LPCAT3 in HK-2 cells treated with 20 ng/mL for 48 h in the presence or absence of Fer-1 (2 μM) for 48 h ($n=3$). The quantification results are shown in the right panel. d, Cell survival was determined with an MTT kit ($n=6$). e, Cytotoxicity was determined with an LDH kit ($n=3$). f, The level of MDA in the indicated groups. All the data are presented as the means ± SDs. *$P<0.05$, **$P<0.005$,***$P<0.001$, ****$P<0.0001$, ns represents no significance. Statistical analysis was performed via two-way analysis of variance (ANOVA) with the Bonferroni post hoc correction.

Supplementary Material 3: Supplementary Figure 3. Ferroptosis in TECs is impaired in GPX4-overexpressing mice during UUO. GPX4-overexpressing and control adenoviruses were injected into the kidney proximal tubules of C57BL/6 mice. Four weeks after UUO surgery, the mice were euthanized at 14 d. a, Representative images ($n=6$) of 4-HNE and GPX4 in mouse kidney sections. Scale bars, 50 μm. b, Immunoblot analysis of the expression of GPX4, ACSL4, and LPCAT3 ($n=3$). For all panels, the data are presented as the means ± SDs. c, Representative images ($n=5$) of renal sections from a mouse kidney on day 14 with AAV-GPX4-OE subjected to TUNEL staining. Scale bars, 50 μm. For all panels, the data are presented as the means ± SDs. *$P<0.05$, **$P<0.005$, ***$P<0.001$,****$P<0.0001$, ns indicates no significance. Statistical analysis was performed via two-way analysis of variance (ANOVA) with the Bonferroni post hoc correction.

Supplementary Material 4: Supplementary Figure 4. Ferroptosis activation in TGF-β-treated HK-2 cells is suppressed by GPX4 overexpression. a, Representative images of 4-HNE immunostaining in HK-2 cells. Scale bars, 50 μm. b, Lipid peroxidation was detected via BODIPY 581/591 C11 staining via confocal microscopy. Scale bars, 50 μm. c, Protein expression (western blot) of GPX4, ACLS4, and LPCAT3 in HK-2 cells treated with 20 ng/mL TGF-β for 48 h with or without GPX4 overexpression for 48 h ($n=3$). The quantification results are shown in the right panel. d, Cell survival was determined with an MTT kit ($n=6$). e, Cytotoxicity was determined with an LDH kit ($n=3$). f, The level of MDA in the indicated groups. All the data are presented as the means ± SDs. *$P<0.05$, **$P<0.005$,***$P<0.001$, ****$P<0.0001$, ns represents no significance. Statistical analysis was performed via two-way analysis of variance (ANOVA) with the Bonferroni post hoc correction.

Acknowledgements

The National Natural Science Foundation of China (NSFC) (grant number 82171575) and the Hubei Provincial Clinical Medical Research Center for Nephropathy (grant number OIR202402Z) were gratefully acknowledged.

Authors' contributions

Y.T.C. and Y.D. performed the experiments. Y.T.C. analyzed the data and wrote the manuscript. Q.Y. conceived the study, prepared the figures, and revised the manuscript. Y.H. and L.Z. supervised the experiments. C.T.Z. contributed analytic tools. H.Y.G. reviewed the manuscript.

Funding

This work was financially supported by grants from the National Natural Science Foundation of China (NSFC) (No. 81800603) and the Hubei Provincial Clinical Medical Research Center for Nephropathy (OIR202402Z).

Data availability

No datasets were generated or analysed during the current study.

Declarations

Ethics approval and consent to participate

This paper does not describe studies involving human participants, human data or human tissue. All animal interventions were approved by the Ethics Committee of Union Hospital, Tongji Medical College, Huazhong University of Science and Technology, China.

Competing interests

The authors declare no competing interests.

Author details

[1]Department of Geriatrics, Tongji Hospital of Tongji Medical College, Huazhong University of Science and Technology, Wuhan 430030, China. [2]Key Laboratory of Vascular Aging, Ministry of Education, Tongji Hospital of Tongji Medical College, Huazhong University of Science and Technology, Wuhan 430030, China. [3]Division of Nephrology, Department of Geriatrics, the First Affiliated Hospital of Nanjing Medical University, Nanjing, Jiangsu 210029, China.

Received: 8 November 2024 Accepted: 28 January 2025
Published online: 11 February 2025

References

1. Webster AC, Nagler EV, Morton RL, Masson P. Chronic kidney disease. Lancet. 2017;389:1238–52. https://doi.org/10.1016/s0140-6736(16)32064-5.
2. Neuen BL, Chadban SJ, Demaio AR, Johnson DW, Perkovic V. Chronic kidney disease and the global NCDs agenda. BMJ Global Health. 2017;2:e000380. https://doi.org/10.1136/bmjgh-2017-000380.
3. Romagnani P, Remuzzi G, Glassock R, Levin A, Jager KJ, Tonelli M, Massy Z, Wanner C, Anders HJ. Chronic kidney disease. Nat Rev Dis Primers. 2017;3:17088. https://doi.org/10.1038/nrdp.2017.88.
4. Liu BC, Tang TT, Lv LL, Lan HY. Renal tubule injury: a driving force toward chronic kidney disease. Kidney Int. 2018;93:568–79. https://doi.org/10.1016/j.kint.2017.09.033.
5. Dixon SJ, Lemberg KM, Lamprecht MR, Skouta R, Zaitsev EM, Gleason CE, Patel DN, Bauer AJ, Cantley AM, Yang WS, et al. Ferroptosis: an iron-dependent form of nonapoptotic cell death. Cell. 2012;149:1060–72. https://doi.org/10.1016/j.cell.2012.03.042.
6. Stockwell BR, Friedmann Angeli JP, Bayir H, Bush AI, Conrad M, Dixon SJ, Fulda S, Gascon S, Hatzios SK, Kagan VE, et al. Ferroptosis: a regulated cell death Nexus linking metabolism, redox biology, and disease. Cell. 2017;171:273–85. https://doi.org/10.1016/j.cell.2017.09.021.
7. Tang D, Chen X, Kang R, Kroemer G. Ferroptosis: molecular mechanisms and health implications. Cell Res. 2020. https://doi.org/10.1038/s41422-020-00441-1.
8. Dai Y, Wei X, Jiang T, Wang Q, Li Y, Ruan N, Luo P, Huang J, Yang Y, Yan Q, et al. Ferroptosis in age-related vascular diseases: molecular mechanisms and innovative therapeutic strategies. Biomed Pharmacother. 2024;173. https://doi.org/10.1016/j.biopha.2024.116356.
9. Sponsel HT, Alfrey AC, Hammond WS, Durr JA, Ray C, Anderson RJ. Effect of iron on renal tubular epithelial cells. Kidney Int. 1996;50:436–44. https://doi.org/10.1038/ki.1996.334.
10. Naito Y, Fujii A, Sawada H, Oboshi M, Iwasaku T, Okuhara Y, Morisawa D, Eguchi A, Hirotani S, Masuyama T. Association between renal iron accumulation and renal interstitial fibrosis in a rat model of chronic kidney disease. Hypertens Res. 2015;38:463–70. https://doi.org/10.1038/hr.2015.14.
11. Ikeda Y, Ozono I, Tajima S, Imao M, Horinouchi Y, Izawa-Ishizawa Y, Kihira Y, Miyamoto L, Ishizawa K, Tsuchiya K, et al. Iron chelation by deferoxamine prevents renal interstitial fibrosis in mice with unilateral ureteral obstruction. PLoS ONE. 2014;9:e89355. https://doi.org/10.1371/journal.pone.0089355.
12. Stockwell BR. Ferroptosis turns 10: emerging mechanisms, physiological functions, and therapeutic applications. Cell. 2022;185:2401–21. https://doi.org/10.1016/j.cell.2022.06.003.
13. Dai Y, Chen Y, Mo D, Jin R, Huang Y, Zhang L, Zhang C, Gao H, Yan Q. Inhibition of ACSL4 ameliorates tubular ferroptotic cell death and protects against fibrotic kidney disease. Commun Biol. 2023;6:907. https://doi.org/10.1038/s42003-023-05272-5.
14. Zhang B, Chen X, Ru F, Gan Y, Li B, Xia W, Dai G, He Y, Chen Z. Liproxstatin-1 attenuates unilateral ureteral obstruction-induced renal fibrosis by inhibiting renal tubular epithelial cells ferroptosis. Cell Death Dis. 2021;12:843. https://doi.org/10.1038/s41419-021-04137-1.
15. Zhu B, Ni Y, Gong Y, Kang X, Guo H, Liu X, Li J, Wang L. Formononetin ameliorates ferroptosis-associated fibrosis in renal tubular epithelial cells and in mice with chronic kidney disease by suppressing the Smad3/ATF3/SLC7A11 signaling. Life Sci. 2023;315. https://doi.org/10.1016/j.lfs.2022.121331.
16. Zhao Z, Wu J, Xu H, Zhou C, Han B, Zhu H, Hu Z, Ma Z, Ming Z, Yao Y, et al. XJB-5-131 inhibited ferroptosis in tubular epithelial cells after ischemia-reperfusion injury. Cell Death Dis. 2020;11:629. https://doi.org/10.1038/s41419-020-02871-6.
17. Seiler A, Schneider M, Förster H, Roth S, Wirth EK, Culmsee C, Plesnila N, Kremmer E, Rådmark O, Wurst W, et al. Glutathione peroxidase 4 senses and translates oxidative stress into 12/15-lipoxygenase dependent- and AIF-mediated cell death. Cell Metab. 2008;8:237–48. https://doi.org/10.1016/j.cmet.2008.07.005.
18. Yang WS, SriRamaratnam R, Welsch ME, Shimada K, Skouta R, Viswanathan VS, Cheah JH, Clemons PA, Shamji AF, Clish CB, et al. Regulation of ferroptotic cancer cell death by GPX4. Cell. 2014;156:317–31. https://doi.org/10.1016/j.cell.2013.12.010.
19. Friedmann Angeli JP, Schneider M, Proneth B, Tyurina YY, Tyurin VA, Hammond VJ, Herbach N, Aichler M, Walch A, Eggenhofer E, et al. Inactivation of the ferroptosis regulator Gpx4 triggers acute renal failure in mice. Nat Cell Biol. 2014;16:1180–91. https://doi.org/10.1038/ncb3064.
20. Zilka O, Shah R, Li B, Friedmann Angeli JP, Griesser M, Conrad M, Pratt DA. On the mechanism of cytoprotection by ferrostatin-1 and liproxstatin-1 and the role of lipid peroxidation in ferroptotic cell death. ACS Cent Sci. 2017;3:232–43. https://doi.org/10.1021/acscentsci.7b00028.
21. Miotto G, Rossetto M, Di Paolo ML, Orian L, Venerando R, Roveri A, Vuckovic AM, Bosello Travain V, Zaccarin M, Zennaro L, et al. Insight into the mechanism of ferroptosis inhibition by ferrostatin-1. Redox Biol. 2020;28:101328. https://doi.org/10.1016/j.redox.2019.101328.
22. Lonn P, Moren A, Raja E, Dahl M, Moustakas A. Regulating the stability of TGFbeta receptors and smads. Cell Res. 2009;19:21–35. https://doi.org/10.1038/cr.2008.308.
23. Kok HM, Falke LL, Goldschmeding R, Nguyen TQ, Targeting CTGF. EGF and PDGF pathways to prevent progression of kidney disease. Nat Rev Nephrol. 2014;10:700–11. https://doi.org/10.1038/nrneph.2014.184.
24. Meng XM, Nikolic-Paterson DJ, Lan HY. TGF-β: the master regulator of fibrosis. Nat Rev Nephrol. 2016;12:325–38. https://doi.org/10.1038/nrneph.2016.48.
25. Chen YT, Jhao PY, Hung CT, Wu YF, Lin SJ, Chiang WC, Lin SL, Yang KC. Endoplasmic reticulum protein TXNDC5 promotes renal fibrosis by enforcing TGF-β signaling in kidney fibroblasts. J Clin Invest. 2021;131. https://doi.org/10.1172/jci143645.
26. Fan X, Zhang X, Liu LC, Zhang S, Pelger CB, Lughmani HY, Haller ST, Gunning WT 3rd, Cooper CJ, Gong R, et al. Hemopexin accumulates in kidneys and worsens acute kidney injury by causing hemoglobin deposition and exacerbation of iron toxicity in proximal tubules. Kidney Int. 2022;102:1320–30. https://doi.org/10.1016/j.kint.2022.07.024.
27. Hu J, Gu W, Ma N, Fan X, Ci X. Leonurine alleviates ferroptosis in cisplatin-induced acute kidney injury by activating the Nrf2 signalling pathway. Br J Pharmacol. 2022;179:3991–4009. https://doi.org/10.1111/bph.15834.
28. Kim S, Kang SW, Joo J, Han SH, Shin H, Nam BY, Park J, Yoo TH, Kim G, Lee P, et al. Characterization of ferroptosis in kidney tubular cell death under diabetic conditions. Cell Death Dis. 2021;12:160. https://doi.org/10.1038/s41419-021-03452-x.
29. Zhang HY, Cheng M, Zhang L, Wang YP. Ferroptosis and renal fibrosis: a new target for the future (review). Exp Ther Med. 2023;25:13. https://doi.org/10.3892/etm.2022.11712.
30. Li S, Han Q, Liu C, Wang Y, Liu F, Pan S, Zuo L, Gao D, Chen K, Feng Q, et al. Role of ferroptosis in chronic kidney disease. Cell Commun Signal. 2024;22:113. https://doi.org/10.1186/s12964-023-01422-8.
31. Jin R, Dai Y, Wang Z, Hu Q, Zhang C, Gao H, Yan Q. Unraveling ferroptosis: a new frontier in combating renal fibrosis and CKD progression. Biology (Basel). 2024;14. https://doi.org/10.3390/biology14010012.

32. Jiang X, Stockwell BR, Conrad M. Ferroptosis: mechanisms, biology and role in disease. Nat Rev Mol Cell Biol. 2021;22:266–82. https://doi.org/10.1038/s41580-020-00324-8.
33. Le Y, Zhang Z, Wang C, Lu D. Ferroptotic cell death: new regulatory mechanisms for metabolic diseases. Endocr Metab Immune Disord Drug Targets. 2021;21:785–800. https://doi.org/10.2174/1871530320666200731175328.
34. Bersuker K, Hendricks JM, Li Z, Magtanong L, Ford B, Tang PH, Roberts MA, Tong B, Maimone TJ, Zoncu R, et al. The CoQ oxidoreductase FSP1 acts parallel to GPX4 to inhibit ferroptosis. Nature. 2019;575:688–92. https://doi.org/10.1038/s41586-019-1705-2.
35. Ingold I, Berndt C, Schmitt S, Doll S, Poschmann G, Buday K, Roveri A, Peng X, Porto Freitas F, Seibt T, et al. Selenium utilization by GPX4 is required to prevent hydroperoxide-induced ferroptosis. Cell. 2018;172(e421):409–22. https://doi.org/10.1016/j.cell.2017.11.048.
36. Wang J, Wang Y, Liu Y, Cai X, Huang X, Fu W, Wang L, Qiu L, Li J, Sun L. Ferroptosis, a new target for treatment of renal injury and fibrosis in a 5/6 nephrectomy-induced CKD rat model. Cell Death Discov. 2022;8. https://doi.org/10.1038/s41420-022-00931-8.
37. Wang Y, Zhang M, Bi R, Su Y, Quan F, Lin Y, Yue C, Cui X, Zhao Q, Liu S, et al. ACSL4 deficiency confers protection against ferroptosis-mediated acute kidney injury. Redox Biol. 2022;51:102262. https://doi.org/10.1016/j.redox.2022.102262.
38. Chu LK, Cao X, Wan L, Diao Q, Zhu Y, Kan Y, Ye LL, Mao YM, Dong XQ, Xiong QW, et al. Autophagy of OTUD5 destabilizes GPX4 to confer ferroptosis-dependent kidney injury. Nat Commun. 2023;14. https://doi.org/10.1038/s41467-023-44228-5.
39. Kim DH, Kim WD, Kim SK, Moon DH, Lee SJ. TGF-beta1-mediated repression of SLC7A11 drives vulnerability to GPX4 inhibition in hepatocellular carcinoma cells. Cell Death Dis. 2020;11:406. https://doi.org/10.1038/s41419-020-2618-6.
40. Zhou L, Xue X, Hou Q, Dai C. Targeting ferroptosis attenuates interstitial inflammation and kidney fibrosis. Kidney Dis (Basel). 2022;8:57–71. https://doi.org/10.1159/000517723.
41. Ide S, Kobayashi Y, Ide K, Strausser SA, Abe K, Herbek S, O'Brien LL, Crowley SD, Barisoni L, Tata A, et al. Ferroptotic stress promotes the accumulation of pro-inflammatory proximal tubular cells in maladaptive renal repair. Elife. 2021;10. https://doi.org/10.7554/eLife.68603.
42. Chung AC, Lan HY. Chemokines in renal injury. J Am Soc Nephrol JASN. 2011;22:802–9. https://doi.org/10.1681/ASN.2010050510.
43. Sedeek M, Nasrallah R, Touyz RM, Hebert RL. NADPH oxidases, reactive oxygen species, and the kidney: friend and foe. J Am Soc Nephrol JASN. 2013;24:1512–8. https://doi.org/10.1681/ASN.2012111112.
44. Prozialeck WC, Edwards JR. Cell adhesion molecules in chemically-induced renal injury. Pharmacol Ther. 2007;114:74–93. https://doi.org/10.1016/j.pharmthera.2007.01.001.
45. Geng H, Lan R, Singha PK, Gilchrist A, Weinreb PH, Violette SM, Weinberg JM, Saikumar P, Venkatachalam MA. Lysophosphatidic acid increases proximal tubule cell secretion of profibrotic cytokines PDGF-B and CTGF through LPA2- and galphaq-mediated rho and alphavbeta6 integrin-dependent activation of TGF-beta. Am J Pathol. 2012;181:1236–49. https://doi.org/10.1016/j.ajpath.2012.06.035.

Publisher's Note